JOURNAL OF AEROSPACE SOCIETY MALAYSIA

ARTICLE

FLEXIBLE WING DESIGN STRUCTURAL PERFORMANCE UNDER STATIC AEROELASTIC CONDITION

Nur Namierah Abdul Aziz[1], Mohammad Yazdi Harmin[1] and Hidayatullah Mohammad Ali[1,*]

1. Department of Aerospace Engineering, Faculty of Engineering, Universiti Putra Malaysia, 43400 Serdang, Selangor, Malaysia

*Correspondence: hidayatullah@upm.edu.my

Abstract: This study investigates the static aeroelastic response of a flexible wing, emphasizing the role of the internal rib configurations in governing the structural deflection and stiffness. With the aerospace industry advancing toward lighter weight, having high-aspect-ratio wings and achieving the structural efficiency without compromising integrity has become a central design challenge. A baseline aluminum wing box was developed using finite element methods, fabricated and experimentally validated through experimental modal analysis (EMA). To improve model accuracy, design sensitivity and optimization (SOL 200) was employed to refine material properties, ensuring close validation between simulated and measured natural frequencies. Using the validated model, multiple rib configurations were evaluated under aerodynamic loading via the linear static analysis (SOL 101) at a fixed angle of attack. The results demonstrate that rib topology strongly influences static aeroelastic behavior. In particular, optimized rib layouts reduced the wingtip deflection and also improved the natural frequencies by up to 13%, indicating enhanced stiffness without added weight. On the whole, findings from this study highlights the potential of rib configuration tailoring as an effective aeroelastic strategy for lightweight aircraft and unmanned aerial systems, advancing the structural optimization practices through the integration of simulation, experimental validation and fabrication.

Keywords: aeroelastic tailoring, aeroelasticity, finite element analysis, flexible wing, rib configuration

1. Introduction

The pursuit of improved aerodynamic efficiency in modern aircraft has driven the adoption of the slender, high–aspect ratio wing (HARW) designs [1]. Although they are aerodynamically advantageous, such configurations also exhibit greater structural flexibility [2], making them susceptible to aeroelastic instabilities such as torsional divergence, large deflections and control surface reversion [3]. Aeroelastic tailoring of the wing, particularly through the rib configuration, has emerged as a promising strategy to enhance stiffness while avoiding significant weight penalties [4].

Aeroelasticity is broadly categorized into static and dynamic phenomena. Static aeroelastic effects include divergence and control reversal whereas dynamic aeroelasticity relates to flutter and limit cycle oscillations [3]. While dynamic aeroelastic instabilities, especially flutter, have been widely studied due to their catastrophic consequences, the static domain has received comparatively less attention despite its strong influence on the wing deflection and load distribution. Prior work has shown that tailoring the internal wing structures can significantly affect aeroelastic response. Patil and Hodges [2] highlighted the importance of geometric nonlinearities in HARWs while Ting et al. [5] applied the finite-element vortex-lattice method to model static aeroelasticity. Krüger et al. [6] further demonstrated that structural tailoring can alleviate aerodynamic loads in demonstrator wings. The rib and spar configurations play a

central role in the tailoring strategies [7]. Stanford [8] introduced bi-level optimization method to refine rib placement, sizing and wing shaping, showing that curved or unconstrained rib arrangements could improve load path efficiency and expand the aeroelastic design space. Othman et al. [4] investigated rib orientations in a rectangular wing box, resulting in the increment of torsional frequency up to 8.5% and flutter speed gains up to 80% as compared to conventional designs. Robinson et al. [9] extended these findings by employing the SpaRib concepts with curvilinear spars and ribs, achieving improved bend–twist coupling and delayed flutter without mass penalties. Locatelli et al. also showed that incorporating curvilinear spars and ribs (SpaRibs) into the wing structures can substantially enhance their structural performance [10]. Related studies have also explored topology optimization of rib–spar layouts [2], rib thickness variations [11] and experimental assessments of the unconventional rib configurations [4, 10], collectively reinforcing the centrality of rib management in aeroelastic tailoring.

Despite these advances, much of the literatures emphasizes flutter or dynamic phenomena, leaving static aeroelastic behavior comparatively underexplored. This gap is critical as static deflection directly affects aerodynamic efficiency, load transfer and structural integrity [2]. To address this, the present study investigates the static aeroelastic response of a flexible aluminum wing with unconventional rib configurations. A validated baseline wing model, established through the experimental modal analysis, serves as the reference for comparison. Building on this foundation, the research evaluates how the rib spacing and the rib count influence both deflection and stiffness under steady aerodynamic loading. By correlating experimental and numerical findings, the study quantifies how rib management can improve the stiffness without any added structural mass. The outcomes provide both fundamental insight into aeroelastic tailoring and practical guidance for lightweight aircraft and unmanned aerial vehicle (UAV). Overall, this work contributes to the aeroelastic tailoring research by shifting the emphasis toward static aeroelastic effects and validating unconventional rib configurations stiffness. The results provide new evidence that the rib spacing and distribution can mitigate deflection, improve stiffness and support the development of efficient high–aspect ratio wing designs.

2. Methodology

This study was conducted in three main phases. Firstly, a baseline wing model was developed and numerically analyzed to establish the reference performance. Secondly, the model was fabricated and validated through the experimental testing to ensure consistency between the physical and numerical models. Finally, static aeroelastic analyses were performed to evaluate the effects of the alternative rib configurations on wing stiffness and deflection. All computational analyses were carried out using MSC Nastran [12], employing the following Solution Sequences (SOL):

(a) SOL 103 (Normal Mode Analysis): to extract natural frequencies and mode shapes
(b) SOL 101 (Linear Static Analysis): to evaluate deflections under aerodynamic loading
(c) SOL 145 (Flutter Analysis): to determine flutter onset speeds
(d) SOL 200 (Design Sensitivity and Optimization): to refine material properties for improved correlation with experimental data

2.1 Structural model

The baseline wing was modeled as a half-wing configuration with an aspect ratio (AR) of 7, two C-shaped spars and eight C-shaped ribs. The structure was modeled in aluminum, which was chosen for its high strength-to-weight ratio and ease of fabrication. The material was assumed homogeneous and isotropic, with Young's modulus of 70 GPa, Poisson's ratio value of 0.35 and density with 2700 kg/m^3. Meshing seed was applied at the model curves and equivalencing the mesh using tolerance cube method

with 0.005 equivalencing tolerance. The spars had dimensions of 0.01 m width, 0.015 m height and 0.001 m thickness while the ribs were measured 0.01 m width, 0.013 m height and 0.001 m thickness. A boundary condition was applied at the wing root, ensuring no rotational or translational movement in the x, y and z axis at the root. Aerodynamic loading was determined using the thin airfoil theory, expressed as Equation 1, where L is lift force, ρ is air density with a constant value of 1.225 kg/m³, V is freestream velocity of 5 m/s to 25 m/s, S is wing strip area and C_L is lift coefficient at angles of attack (AOA) of 2° and 10°.

$$L = \frac{1}{2}\rho V^2 S C_L \tag{1}$$

The loads were distributed along the front spar using the strip method as indicated in Figure 1. A Linear Static Analysis (SOL 101) was conducted to assess the deflections under aerodynamic loading, with the maximum deflection constrained to 0.3 m based on the wind tunnel limitations. Flutter analysis (SOL 145) was also performed to confirm flutter onset within 20 m/s to 25 m/s. If these conditions were not met, the span and chord dimensions were adjusted, and the process was repeated. The finalized configuration, which satisfied both structural and also aeroelastic criteria, was established as the baseline wing model**.**

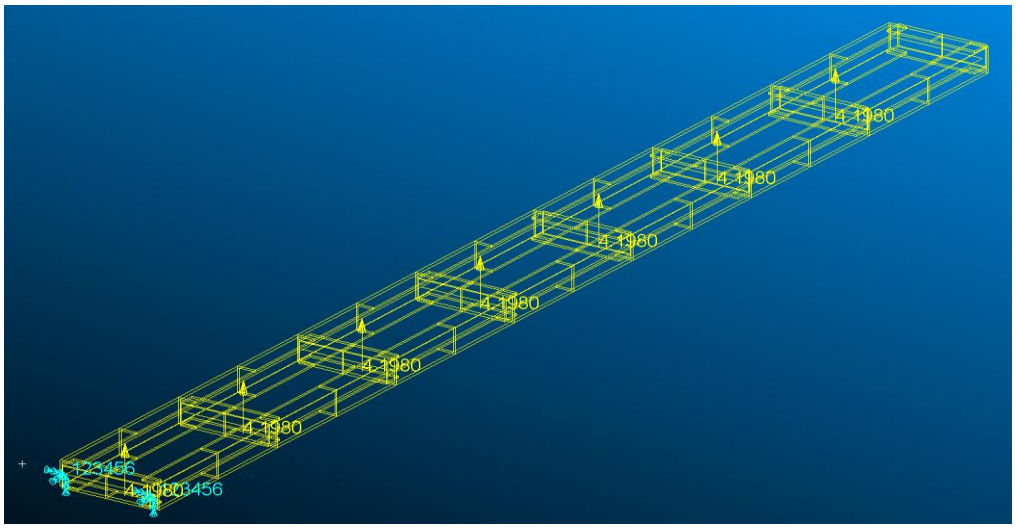

Figure 1: Loads applied on front spar

2.2 Fabrication and experimental validation

The baseline wing box was fabricated using T6 aluminum sheets of 0.001 m thickness. Metal sheets were cut to dimension using a cut-off machine, bent into C-shaped profiles and assembled with rivets following the detailed CAD drawings and assembly guides. A 4-cm spar extension was included for the clamping purposes. The completed wing box was covered with a curved styrofoam surface to represent the aerodynamic profile.

A custom clamp was designed using CAD and 3D-printed in PLA with 80% infill density to secure the wing root during testing. This ensured the boundary conditions were consistent with the FE model. The fabricated wing box underwent experimental modal analysis (EMA) using roving impact hammer test as displayed in Figure 2. Accelerometers were mounted spanwise and impact excitation was applied at multiple points. The frequency response functions (FRFs) were recorded, which were then processed

to extract natural frequencies and mode shapes. These were compared with FEA results to validate the baseline model.

Figure 2: Experimental modal analysis (EMA) setup

Upon validation, SOL 200 iteratively adjusts the Young's Modulus, Poisson's ratio and also density. This solution sequence performs design sensitivity analysis and automated optimization to identify the most suitable material property set, in which the boundary range applied is the properties current values. The solver then iteratively adjusts these variables, whereby the optimized values are then applied in the model and the Normal Mode Analysis (SOL 103) is performed. The revised natural frequencies are extracted and compared against both the original simulation results and the experimental data to verify improvement. The optimized material properties are subsequently applied in the following stages of the project, including the static analysis of modified rib configurations.

2.3 Rib configuration analysis

Two categories of rib modifications were examined in this study, which included non-uniform rib spacing and rib count variation. For non-uniform spacing, two models with eight ribs were developed, one with increasing spacing from 6 cm at the root to 18 cm at the tip as depicted in Figure 3a, and one with decreasing spacing from 18 cm at the root to 6 cm at the tip as in Figure 3b. Two additional configurations were created with 10 ribs as presented in Figure 4a and 12 ribs in Figure 4b, uniformly spaced across the span. Loads identical to the baseline model were applied using the strip theory at 10° AOA and velocities of 5, 10, 15, 20 and 25 m/s**.** A Linear Static Analysis (SOL 101) was conducted to evaluate deflection responses.

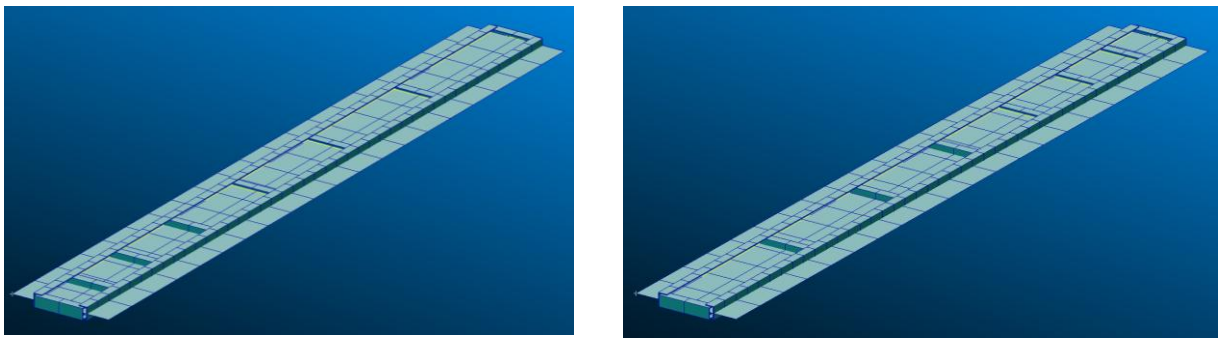

(a) Increasing spacing (b) Decreasing spacing

Figure 3: Models with varying spacing

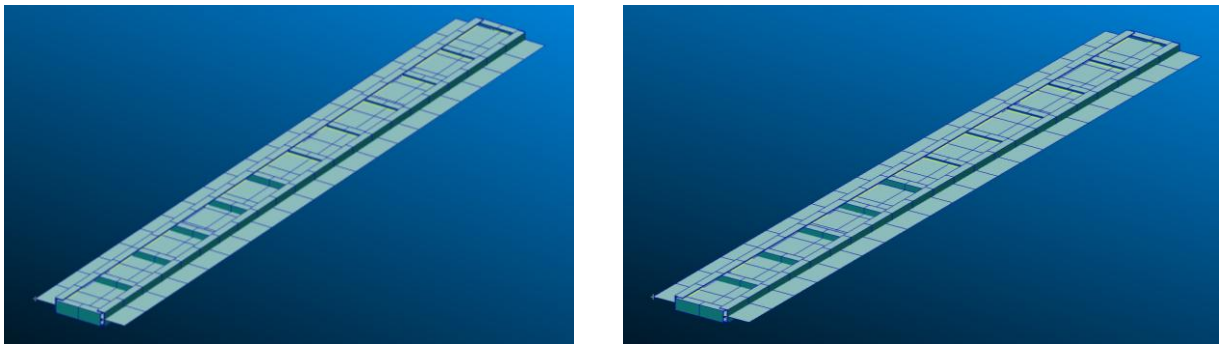

(a) 10 ribs (b) 12 ribs

Figure 4: Models with varying ribs number

The configuration yielding the lowest deflection was further analyzed using Normal Mode Analysis (SOL 103) to extract natural frequencies and mode shapes. The percentage differences relative to the baseline were calculated to evaluate stiffness improvements. The configuration with the best combined performance in static and modal analyses was selected as the optimal rib arrangement for this study.

3. Results and Discussion

The results are organized into three parts: baseline wing development, experimental validation and analysis of the unconventional rib configurations. Numerical and experimental findings are integrated to demonstrate how the rib layout influences the wing deflection and stiffness under static aeroelastic conditions.

3.1 Baseline design development

Five half-wing designs, each with an aspect ratio of seven and eight ribs, were initially evaluated to identify the suitable baseline configuration. The selection was guided by two performance constraints: a maximum wingtip deflection of 0.3 m and a flutter onset speed not exceeding 25 m/s, consistent with the dimensional and operational limitations of the closed-loop wind tunnel test section of 1 m × 1 m × 3 m. Each design was subjected to Linear Static Analysis (SOL 101) at the angles of attack (AOA) of 2° and 10°. The translational deflections were found to be consistently lower and also very minimal than rotational deflections. Given the negligible effect, it can be omitted in this discussion for clarity and simplicity. Among the designs, the half wing with span 0.63 m and chord length of 0.09 m had demonstrated the lowest deflection of 0.03 m while the half wing with span 0.84 m and chord length of 0.12 m exhibited the highest, reaching 0.28 m at 10° AOA and 25 m/s. Despite this, all designs remained within the allowable limit. Nevertheless, the trend confirmed that increasing span leads to higher deflections due to reduced stiffness**.**

Flutter performance was assessed using SOL 145, only half wing with span of 0.84 m and chord length of 0.12 m satisfied the flutter constraint, with onset occurring at 21.3 m/s. This result indicated that while longer spans increased deflection, they also shifted flutter onset to higher speeds, reflecting increased structural rigidity. Based on compliance with both criteria, the half wing with span of 0.84 m and chord length of 0.12 m was selected as the baseline model**.** A Normal Mode Analysis (SOL 103) was subsequently performed to extract the natural frequencies and mode shapes.

3.2 Baseline model validation

The fabricated baseline wing box was validated experimentally through experimental EMA using the roving impact hammer test. The resulting FRFs enabled extraction of natural frequencies and mode shapes. A comparison between simulated and experimental frequencies is presented in Table 1.

Table 1: Frequencies from EMA and FEA

Mode	EMA Natural Frequency (Hz)	FEA Natural Frequency (Hz)	Percentage Error (%)
1	14.6722	20.9699	42.92
2	38.5121	33.8300	12.16
3	110.0344	130.3570	18.47
4	157.2872	157.4560	0.11
5	312.8636	361.0750	15.41
6	385.5028	407.1590	5.62

Comparisons between the simulated and the experimental natural frequencies showed significant deviations in bending modes. Mode 1 exhibited a 42.92% error while Mode 3 and Mode 5 deviated by 18.47% and 15.41%, respectively. Torsional modes from Modes 2, 4 and 6 displayed smaller percentage errors, suggesting that the torsional stiffness was better captured in the simulation. The percentage error may be attributed to the fabrication imperfections from the model fabrication material offset, which is the Aluminum 6061-T6, and also the experimental variations such as model experimental orientation and the styrofoam on the spars acting as a damper, which lowers the measured natural frequency.

To improve the validation, Design Sensitivity and Optimization Analysis (SOL 200) was conducted by adjusting Young's modulus, Poisson's ratio and density within defined bounds to refine the model properties. The updated properties are optimized at Young's Modulus of 6.0138×10^{10}, Poisson ratio of 0.05233 and density of 3106.9895 kg/m³, which were then applied to the baseline model and updated frequencies were obtained as presented in Table 2. Although the optimized Poisson's ratio differs from standard aluminum values of 0.3 [12], its use in this study is strictly limited to improving the correlation between the FEA and the EMA.

Table 2: Frequencies from EMA and updated baseline FEA

Mode	EMA Natural Frequency (Hz)	FEA Natural Frequency (Hz)	Percentage Error (%)
1	14.6722	18.19	23.98
2	38.5121	30.43	20.99
3	110.0344	113.16	2.84
4	157.2872	138.53	11.93
5	312.8636	313.79	0.30
6	385.5028	355.49	7.79

The updated model showed improved correlation in the bending modes while torsional frequencies deviated slightly more, suggesting an enhanced flexural stiffness but reduced torsional stiffness. On average, the percentage error decreased to approximately 23%. Despite remaining discrepancies, largely

attributed to the fabrication imperfections in Aluminum 6061-T6, minor cracking during forming and damping from the Styrofoam fairings, the experimental results had validated the baseline as sufficiently accurate for further analysis. Importantly, the mode shapes remained consistent across simulations and experiments, confirming structural accuracy.

3.3 Static analysis of unconventional rib configurations

With the validated model established, alternative rib configurations were examined to determine their influence on static performance. Two unconventional designs were first considered, one with rib spacing increasing toward the tip and another with spacing decreasing toward the tip, each with eight ribs. Deflection responses at 10° AOA and across velocities of 5 to 25 m/s are shown in Figure 5**.**

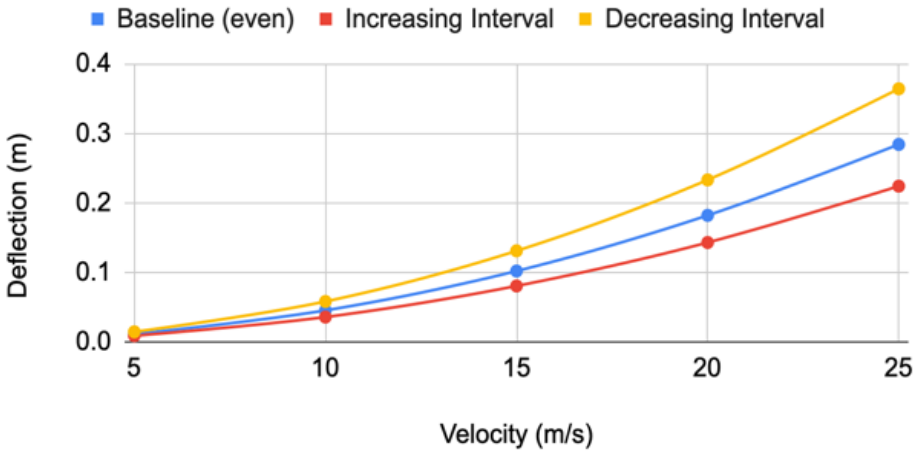

Figure 5: Effect of rib spacing on rotational deflection

The optimized baseline exhibited higher rotational deflections than the original baseline, with the values of 0.288 m at 25 m/s, consistent with reduced stiffness indicated by lower natural frequencies. Among the new configurations, the increasing rib spacing model performed best, recording 0.224 m of deflection at 25 m/s. In contrast, the decreasing spacing design performed worse, with 0.364 m. These results highlighted the role of rib spacing in distributing the load transfer and stiffness, where evenly distributing load paths increases stiffness while clustering the ribs near the root decreases the structural efficiency.

Figure 6 displays the deflection responses for different rib counts with equal spacing. The graph indicates that an increase in the number of ribs corresponds to greater deflection. An increased number of ribs at 10, which is additional of 2 ribs from the baseline, deflects at 0.359 m in rotational deflection at 25 m/s. While for 12 ribs, an addition of 4 ribs to the baseline, also shows an increase on deflection with torsional deflection at 0.426 m. This suggests that a higher rib count reduces the overall stiffness of the structure, which can be attributed to the additional weight introduced by the extra ribs.

Table 3 and Table 4 tabulate the results of the Normal Mode Analysis (SOL 103) on the best rib configuration, which is the increasing spacing. Table 3 shows an average improvement of 13.66% in natural frequencies compared to the baseline, across both bending and torsional modes. Table 4 shows the rotational deflection is reduced by approximately 22% across all modes, demonstrating enhanced

torsional rigidity. On the whole, the results validate the increasing-spacing configuration as the optimal rib arrangement, offering enhanced stiffness.

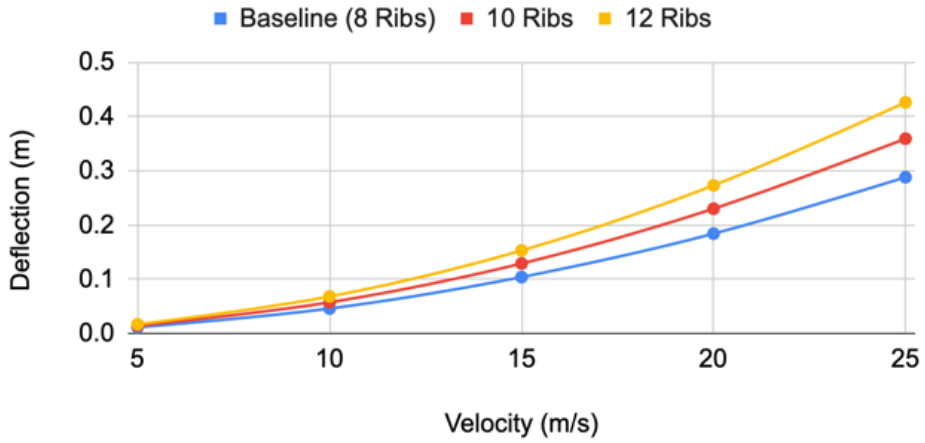

Figure 6: Effect of number of ribs on rotational deflection

Table 3: Comparison of baseline and optimized natural frequency

Mode	Baseline Natural Frequency (Hz)	Optimized Natural Frequency (Hz)	Improvement (%)
1	18.19	21.52	18.31
2	30.43	33.31	9.46
3	113.16	131.59	16.29
4	138.53	154.047	11.20
5	313.79	361.12	15.08
6	355.49	396.83	11.63

Table 4: Comparison of baseline and optimized rotational deflection

Velocity (m/s)	Baseline Deflection (m)	Optimized Deflection (m)	Improvement (%)
5	0.01	0.01	22.17
10	0.05	0.04	22.17
15	0.10	0.08	22.60
20	0.18	0.14	22.28
25	0.29	0.22	22.22

The analyses confirmed that both rib spacing and rib count significantly influence the stiffness and deflection. The study validated the hypothesis that aeroelastic tailoring through the rib management can enhance the structural performance without increasing mass**.** The results also highlight that increasing rib spacing toward the tip improves stiffness and reduces deflection while increasing rib count reduces stiffness due to the added weight. These findings provide practical guidance for structural optimization of lightweight, high-aspect-ratio wings, reinforcing the importance of rib topology in aeroelastic design.

4. Conclusion

This study investigated the structural performance of the flexible wing under the static aeroelastic conditions, focusing on rib configuration effects. A baseline aluminum wing box with eight C-shaped ribs and two spars was developed using FEA, fabricated and validated through EMA. The experimental natural frequencies and mode shapes showed a good agreement with the simulations, confirming the accuracy of the numerical model. Modified rib layouts demonstrated that rib topology critically affects the structural response, with an average improvement of natural frequency up to 13.66% in comparison with the baseline performance, confirming that rib management enhances structural stability without additional weight, offering a lighter aircraft and improved performance. Moving forward, future work should address dynamic aeroelastic phenomena, explore advanced rib topologies and perform wind tunnel validation for broader application. In conclusion, strategic rib spacing and distribution provide a simple yet effective strategy of improving stiffness and structural efficiency, contributing to more sustainable high-aspect-ratio wing designs.

Acknowledgement

The authors gratefully acknowledge the guidance and encouragement of their supervisors, whose expertise was invaluable to the completion of this work. Appreciation is also extended to all individuals who contributed directly or indirectly to this study. Finally, the authors extend their appreciation to the broader community of researchers and practitioners who will benefit from these findings.

References

[1] Y. Ma, S. Karpuk and A. Elham, 'Conceptual Design and Comparative Study of Strut-Braced Wing and Twin-Fuselage Aircraft Configurations with Ultra-High Aspect Ratio Wings', Aerospace Science and Technology, vol. 121, p. 107395, 2022.

[2] S. Kilimtzidis and V. Kostopoulos, 'Multidisciplinary Structural Optimization of Novel High-Aspect Ratio Composite Aircraft Wings', Structural and Multidisciplinary Optimization, vol. 66, no. 7, 150, 2023.

[3] J. Čečrdle, Whirl Flutter of Turboprop Aircraft Structures. Woodhead Publishing, 2015.

[4] M. Y. Harmin, M. S. Othman, F. I. Romli, 'Parametric Study on the Flutter Characteristics of a Simple Rectangular Wing-Box Model with Varying Ribs Orientation', International Journal of Pure and Applied Mathematics, vol. 119, no. 15, pp. 3771–3777, 2018.

[5] E. Ting, N. T. Nguyen and K. V. Trinh, 'Static Aeroelastic and Longitudinal Trim Model of Flexible Wing Aircraft using Finite-Element Vortex-Lattice Coupled Solution', Proceedings of AIAA/ASME/ASCE/AHS/ASC Structures, Structural Dynamics and Materials Conference, Natural Harbor, USA, January 2014.

[6] W. R. Krüger, Y. M. Meddaikar, J. K. S. Dillinger, J. Sodja and R. De Breuker, 'Application of Aeroelastic Tailoring for Load Alleviation on a Flying Demonstrator Wing', Aerospace, vol. 9, no. 10, p. 535, 2022.

[7] United States Department of Transportation. (2023). FAA-H-8083-31B Aviation Maintenance Technician Handbook – Airframe [Online]. Retrieved from https://www.faa.gov/regulations_ policies/handbooks_manuals/aviation/FAA-H-8083-31B_Aviation_Maintenance_ Technician_ Handbook.pdf

[8] B. Stanford, 'Shape, Sizing and Topology Design of a Wingbox Under Aeroelastic Constraints', Journal of Aircraft, vol. 58, no. 6, pp. 1406-1415, 2021.

[9] J. H. Robinson, J. T. Allison and R. J. Seethaler, 'Aeroservoelastic Optimization of Wing Structure using Curvilinear Spars and Ribs (SPARIBS)', Proceedings of 12th AIAA/ISSMO Multidisciplinary Analysis and Optimization Conference, Washington DC, USA, June 2016.

[10] L. Meng, J. Zhang, Y. Hou, P. Breitkopf, J. Zhu and W. Zhang, 'Revisiting the Fibonacci Spiral Pattern for Stiffening Rib Design', International Journal of Mechanical Sciences, vol. 246, p. 1081312023, 2023.

[11] R. F. Latif, M. K. A. Khan, A. Javed, S. I. A. Shah and S. T. I. Rizvi, 'A Semi-Analytical Approach for Flutter Analysis of a High-Aspect-Ratio Wing', The Aeronautical Journal, vol. 125, no. 1284, pp. 410–429, 2021.

[12] A. P. Mouritz, Introduction to Aerospace Materials. Woodhead Publishing, 2012.

[13] W. Rodden and E. Johnson, MSC/NASTRAN Aeroelastic Analysis User's Guide. The MacNeal-Schwendler Corporation, 1994.